Technical University of Denmark

DTU

Analytical and numerical investigation of bolted steel ring flange connection for offshore wind monopile foundations

Madsen, C.A.; Kragh-Poulsen, Jens-Christian; Tage, K.J.; Andreassen, Michael Joachim

Link back to DTU Orbit

DTU Library
Technical Information Center of Denmark

PAPER • OPEN ACCESS

Analytical and numerical investigation of bolted steel ring flange connection for offshore wind monopile foundations

To cite this article: C A Madsen *et al* 2017 *IOP Conf. Ser.: Mater. Sci. Eng.* **276** 012034

View the article online for updates and enhancements.

Related content

- Prediction of dynamic strains on a monopile offshore wind turbine using virtual sensors
A N Iliopoulos, W Weijtjens, D Van Hemelrijck et al.

- Fatigue reassessment for lifetime extension of offshore wind monopile substructures
Lisa Ziegler and Michael Muskulus

- The Hurst Exponent as an Indicator of the Behaviour of a Model Monopile in an Ocean Wave Testing Basin
Vikram Pakrashi, Richard O'Shea, Vesna Jaksic et al.

Analytical and numerical investigation of bolted steel ring flange connection for offshore wind monopile foundations

C A Madsen[1]*, **J-C Kragh-Poulsen**[2], **K J Thage**[3] a**nd M J Andreassen**[4]

[1,2] COWI A/S, Department of Marine & Foundation Engineering, Parallelvej 2, DK-2800 Kgs. Lyngby, Denmark
[3]COWI A/S, Department of Major Bridges International, Parallelvej 2, DK-2800 Kgs. Lyngby, Denmark
[4]Technical University of Denmark, Department of Civil Engineering, Brovej, Building 118, DK-2800 Kgs. Lyngby, Denmark

*Contact author: chan@cowi.com

Abstract. The monopile foundation is the dominant solution for support of wind turbines in offshore wind farms. It is normally grouted to the transition piece which connects the foundation to the turbine. Currently, the bolted steel ring flange connection is investigated as an alternative. The monopile--transition piece connection has specific problems, such as out-of-verticality and installation damage from driving the MP into the seabed and it is not fully known how to design for these. This paper presents the status of the ongoing development work and an estimate of what still needs to be covered in order to use the connection in practice. This involves presentation of an analytical and non-linear FE analysis procedure for the monopile-transition piece connection composed of two L flanges connected with preloaded bolts. The connection is verified for ultimate and fatigue limit states based on an integrated load simulation carried out by the turbine manufacturer.

1. Introduction

Monopile foundations are the prevailing substructure for offshore wind turbine generators (WTG) supporting 81% of the WTGs in operation at the end of 2016 [1]. The monopile (MP) substructure consists of circular steel tubes welded together and driven to target penetration by hydraulic hammering. The bottom of the WTG tower section is bolted directly to the MP or to the top of the transition piece (TP) by the use of flanges pre-welded to the tubular shells. The majority of the installed MPs have a TP, as shown in Figure 1. The loads between the MP and TP are typically transferred by a grouted connection. Settlements of the TP on several offshore wind farms (OWF) in 2010 [2] with the traditional cylindrical grouted connection led to the development of today's most widely used conical grouted connection and alternatives such as the bolted ring flange connection or slip/double slip joints. Current tendencies are that an increased number of offshore wind farms are moving towards the bolted flange solution between the MP-TP [3].
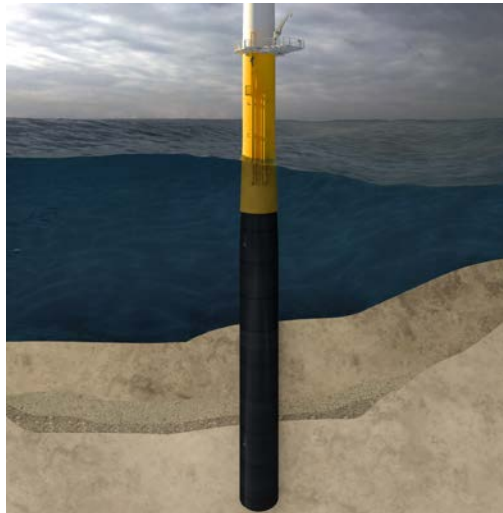
Figure 1. Conceptual sketch of the MP foundation incl. a TP joined to the bottom of the WTG tower. The top of the monopile is joined to the transition piece and the bottom of the monopile is fixed in the seabed. Figure: © COWI A/S.

This paper presents the ongoing work of extending the established design procedures of the bolted steel ring flange connection for the WTG tower to the requirements of the MP-TP connection. The WTG tower flange is typically located as shown in 0, pos. A-D. The position of the MP-TP connection, pos. E, leads to specific considerations of the MP-TP flange connection:

▪ During installation the MP is driven into the seabed by direct hammering on the pile top. This may cause deformation of the flange exceeding limiting values not taken into account in established design procedures.

▪ Driving the MP into the seabed can result in the MP not being perfectly vertical and the WTG mounting flange being inclined. This is not covered in existing design procedures.
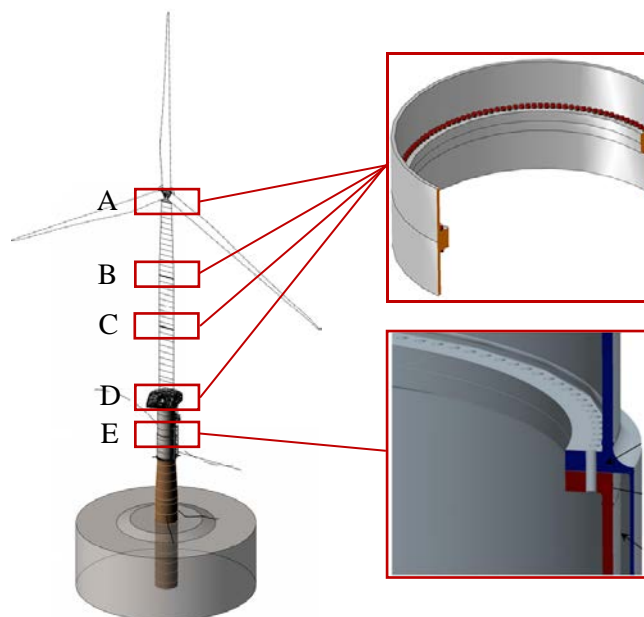

Figure 2. Conceptual and idealized sketch of the MP-TP foundation indicating potential positions for application of a bolted steel ring flange connection. Figure: © COWI A/S.

The work described in this paper is limited to investigation of the ultimate (ULS) and fatigue (FLS) limit states of the flange connection during operation of the WTG. ULS and FLS are investigated by well-known analytical methods considering the shells and the two flanges of the MP-TP. The analytical analysis is accompanied by definition of similar numerical models. This is done to compare the methods and to gain further knowledge of the safety levels included in the analytical approach. An ideal MP-TP flange geometry is assumed in the numerical study, and local and global tolerances are not considered. ULS and FLS loads applied for the investigation are obtained from an offshore wind farm designed by COWI A/S.

2. Analytical approach

The tensile ULS and FLS resistance of the circular flange connection used in present paper are approximated by the analytical methods of Petersen-Seidel and Schmidt-Neuper [4]-[6]. The methods have already been studied by several researchers in relation to the design of the WTG tower or similar tubular flange connections. The review presented in the following, highlights the existing methods and assumptions. Furthermore, it will form the basis for evaluating the key issues associated with the specific requirements of the MP-TP connection.
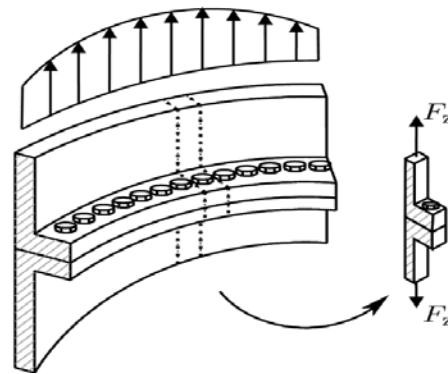

Figure 3. Bolted ring flange connection and equivalent
single bolt segment. Figure from [7].

2.1. Ultimate limit state

The tensile ULS resistance of the flange connection by Petersen and Seidel consider a segment cut out of the entire flange connection (L segment) including a single bolt, see Figure 3. The approach assume linear bolt-load behaviour as preload is not considered. Furthermore, perfectly aligned flanges are assumed.

The L segment is investigated for the equivalent tensile normal force, F_z specified in Equation (1). The expression is derived from Navier's formula considering the foundations global bending moment, M_{Ed} and axial force, N_{Ed} at the position of the circular flange connection. Additional verification is needed for torsional and shear forces which are not considered in present paper. The loads are scaled to the L segment by the number of bolts, n_b in the flange connection and the mid-thickness diameter, $D_{sh,m}$ of the tubular shells.

$$F_z = \frac{4 \cdot M_{Ed}}{n_b \cdot D_{sh,m}} + \frac{N_{Ed}}{n_b} \qquad (1)$$

The tensile resistance of the L segment, $F_{ult,}$ Equation (2) is found from static force equilibrium considering the three failure modes defined in Figure 4.

$$F_z \leq F_{ult} = min(F_{U,A} \; ; \; F_{U,B} \; ; \; F_{U,C1} \; ; \; F_{U,C2}) \qquad (2)$$
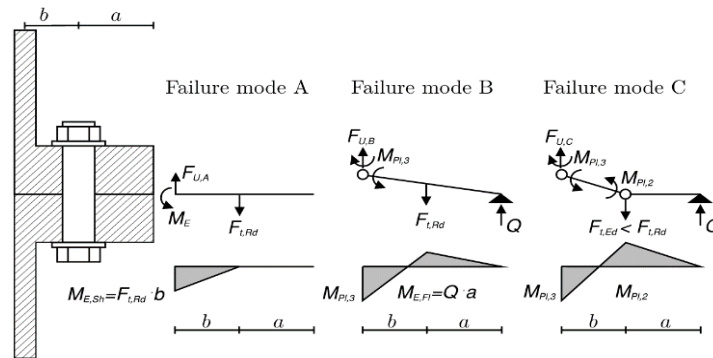
Figure 4. Approximated failure modes for L flange (segment) connection
according to Petersen's method [5]. Figure modified from [7].

2.1.1 Failure of the bolt: The tensile resistance for failure mode A is linked to tensile failure of the bolt. The bending deformation of the flange caused by the eccentric tensile load is assumed small combined with the assumption of a sufficiently large flange thickness resulting in absence of prying forces, Q. The resistance of the segment flange for failure mode A, $F_{U,A}$ is therefore equal to the design tensile resistance of the bolt, $F_{t,RD}$ according to Equations (3) and (4). $f_{y,bolt}$ and $f_{u,bolt}$ is the design yield and ultimate tensile strength of the bolt. A_s is the tensile stress area of the bolt and γ_{M2} and γ_{M7} partial safety factors.

$$F_{U,A} = F_{t,Rd} \tag{3}$$

$$F_{t,Rd} = \min\left(\frac{f_{y,bolt} \cdot A_s}{\gamma_{M2}} ; \frac{0.9 \cdot f_{u,bolt} \cdot A_s}{\gamma_{M7}} \right) \tag{4}$$

Failure mode A assumes that the shell is able to resist the moment, $M_{E,Sh}$ according to Equation (5),

$$\frac{M_{E,Sh}}{W_{E,Shell}} < f_{yd,Shell} \tag{5}$$

where $W_{E,Shell}$ is the elastic moment of resistance and $f_{yd,Shell}$ the design yield strength of the shell.

2.1.2 Failure of the bolt combined with plastic hinge (partial yielding) of the shell: Failure mode B considers combined failure due to plastic yielding of the shell and failure of the bolt in tension. The resistance is obtained from force equilibrium according to Equation (6) assuming the flange can resist the moment, $M_{E,Fl}$ Equation (7).

$$F_{U,B} = \frac{F_{t,Rd} \cdot a + M_{pl,3}}{a + b} \tag{6}$$

$$M_{E,Fl} \leq W_{E,Flange} \cdot f_{yd,Flange} \tag{7}$$

2.1.3 Plastic hinge in shell and flange: Failure mode C examines the tensile resistance, $F_{U,C}$ for the occurrence of failure of the shell and flange due to yielding. This supposes that the considered bolt has sufficient capacity to resist the axial tension load, $F_{t,Ed}$ including effects of prying forces. The resistance is determined from Equation (8). Petersen's method outlined in [5] is different from [4] as it further divides failure mode C into (C1) plastic hinge in the bolt hole center plane and (C2) plastic hinges next to the bolt hole.

$$F_{U,C} = \frac{M_{pl,2} + M_{Pl,3}}{b} \tag{8}$$

2.2. Fatigue limit state

The FLS verification of the circular flange connection is in this paper limited to investigating the resistance of the bolts. The Schmidt-Neuper method [4] links the cyclic load in the form of a max./min. equivalent normal force in the shell, $F_{z \, (max/min)}$ to the bolt force, F_b. The stress range in the bolt is determined from the bolt force from which the fatigue capacity of the bolt can be calculated. The method is selected as it considers the effect of preload and resilience of the joint. The method, however, does not consider bending stresses in the bolt which are taken into account during selection of the fatigue reference strength (FAT class) for the bolt. The Schmidt-Neuper method is devised to be valid for fabrication/installation imperfections of the flange within the specified range defined in Table 1 and illustrated in Figure 5. This implies that the bolt loads determined by the Schmidt-Neuper method include additional prying forces as a consequence of the gap, k. Furthermore, it is assumed that additional bending stresses in the bolts due to the inclination of the flange, α_s are sufficiently small.

The Schmidt-Neuper method approximates the non-linear relation between the shell and bolt forces due to preload by a piecewise trilinear function. The three straight lines are derived by Equations (10)-(12) and presented in Figure 6 as three regions:

Region 1: The bolt load for region 1, $F_{b1,}$ Equation (10) is determined for the flange zone under compression due to the preload. During the increase of the shell load the compressive zone moves in the direction of the edge of the flanges. The bolt load is for region 1 a function of the tensile shell force multiplied by the load factor for the total stiffness of the bolt, p.
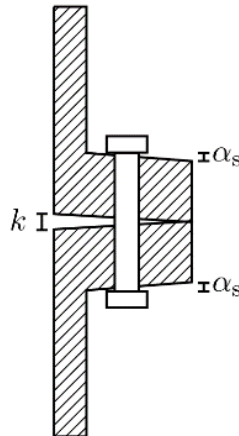
Figure 5. Specification of flange tolerances. Figure from [9].

Table 1. Allowable flange tolerances. According to [9].

Criteria	Limiting value
Flatness deviation, k per flange around the entire circumference	2.0 mm
Flatness deviation, k per flange over a segment of 30°	1.0 mm
Taper, α_s to the inside of the connecting surface of each flange	0.0° to 0.7°
Outer flange surfaces limit, α_s	2°

The preload, $F_{P,C*}$ is added, representing the initial condition before the external load is imposed on the joint. As a consequence, the bolt force relative to the shell force increases in region 1 according to the total stiffness of the joint.

$$F_{b1} = F_{P,C*} + p \cdot F_Z \qquad (9)$$

Region 2: The tensile zone increases in region 2 and the flange connection begins to open, leading to the bolt load, F_{b2} given by Equation (10), to increase more rapidly than the shell force. The first part of Equation (10) represents the maximum bolt force for region 1, and the last part the increase in magnitude of the bolt force relative to the increase in shell force.

$$F_{b2} = F_{P,C*} + p \cdot F_{Z,I,\max} +$$
$$\left[\lambda^* \cdot F_{Z,II,\max} - (F_{P,C*} + p \cdot F_{Z,I,\max}) \right] \cdot$$
$$\frac{Fz - F_{Z,I,\max}}{F_{Z,II,\max} - F_{Z,I,\max}} \tag{10}$$

Region 3: Region 3 is where the tensile shell load has exceeded the compressive preload, $F_{z,IImax}$ and the flanges are in contact only at their edges. The bolt force, F_{b3} given by Equation (11), increases as a function of the shell force multiplied by the auxiliary parameter λ* (16). λ* represents the additional contribution from prying forces due to eccentric load of the connection.

$$F_{b3} = \lambda^* \cdot F_Z \tag{11}$$

It is decided in the present paper to reduce the characteristic preload, $F_{p,C}$ to 90% according to [8], see Equation (12), to account for relaxation of the connection. Assuming a 90% reduction requires re-tightening of the bolts 6 months after commissioning. The torque applied to the bolt should minimum be 70% of the ultimate tensile strength of the bolt.
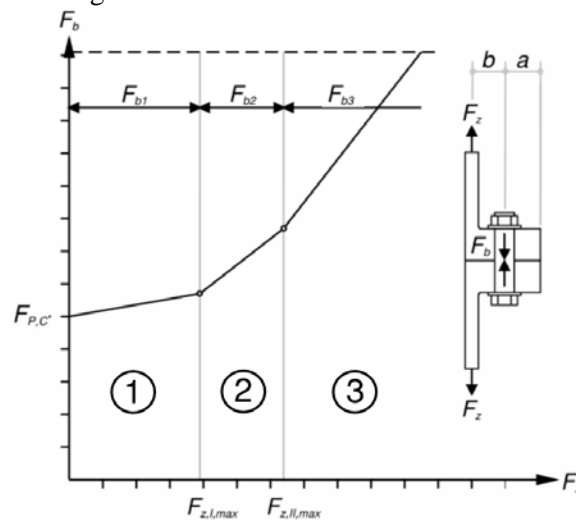
Figure 6. Trilinear approximation of the non-linear relation between
the shell force and the bolt force. Figure modified from [7].

$$F_{P,C*} = 0.7 \cdot A_s \cdot f_{u,bolt} \cdot 0.9 \tag{12}$$

The maximum limit shell force for region 1 and 2 is given in Equations (13) and (14).

$$F_{Z,I,\max} = \frac{a - 0.5 \cdot b}{a + b} \cdot F_{P,C*} \tag{13}$$

$$F_{Z,II,\max} = \frac{1}{\lambda^* \cdot q} \cdot F_{P,C*} \tag{14}$$

$$\lambda^* = \frac{0.7 \cdot a + b}{0.7 \cdot a} \tag{15}$$

The load factor for the total stiffness of the bolt, p, and the flanges, q, are obtained from Equation (16) and (17) where C_s and C_D is the spring stiffness of the tension- and compression spring. δ_P and δ_s represents the elastic resilience of the clamped parts and the bolt. The spring characteristics of the members in the connection are derived according to methods outlined in [10].

$$p = \frac{C_s}{C_S + C_D} \quad q = \frac{C_D}{C_S + C_D} \tag{16}$$

$$C_S = \frac{1}{\delta_s} \qquad C_D = \frac{1}{\delta_p} \tag{17}$$

3. Numerical approach

The ULS and FLS resistance of the one bolt segment is in the present paper investigated by using Abaqus CAE. A geometry equivalent to the analytical approaches presented in Section 2.1 and 2.2 is used and no tolerances are included. Non-linear material properties are defined for the shell, flange, and bolt assembly along with contact interaction specified between the parts according to Table 2. The bolt and nut geometry is simplified where an equivalent shank diameter is specified for the bolt. Linear brick elements (C3D8R) are assigned to the geometry. Different element sizes are used as part of the refinement study. Two types of loads are defined, see Figure 7; a bolt load representing the preload and a pressure load applied at the TP shell representing the equivalent normal force.

The mechanical boundary conditions specified for the L flange segment are shown in Figure 8. This includes cylindrical symmetry conditions applied on both sides of the section cut of the segment and a pinned support at the bottom of the MP shell.

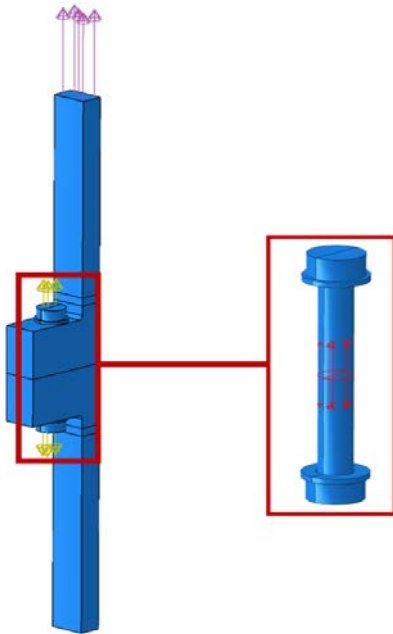**Figure 7.** Definition of loads. Left: Bolt load. Right: Segment shell load. Figure from [7].
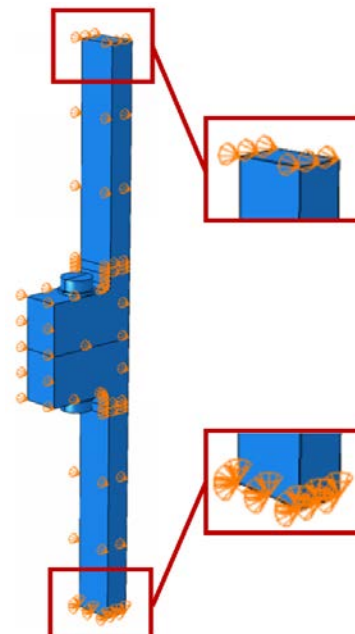
Figure 8. Mechanical boundary conditions specified for the segment model. Left: Pinned support. Right: Cylindrical symmetry condition. Figure from [7].

Table 2. Contact surface properties.

Definition	Flange to flange, Bolt to washer Flange to washer
Friction coefficient	0.2
Behaviour	Small sliding
Formulation	Augmented Lagrange
Interface treatment	Adjust to remove overclosure

4. Case study

The connection is designed as a one sided preloaded flange connection located on the inside of the foundation structure. The connection has 140 bolts specified as hot dip galvanized M64, 10.9 grade (HV M64-10.9 tZn) bolts. The bolt size exceeds M36, hence [11] is consulted for specification of the geometry of the bolt, nut and washer. The flange and shell are specified as S355ML. No tolerances are included in the case study. Non-linear material properties are estimated based on values defined in [12].

4.1. Joint geometry and material parameters

The main geometrical and material parameters of the connection are defined in Figure 9 and listed in Table 3. The material properties including strain hardening, considered in the numerical analysis, are given in Figure 10.
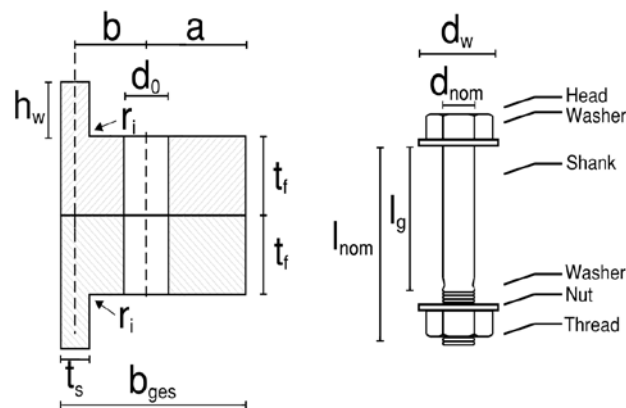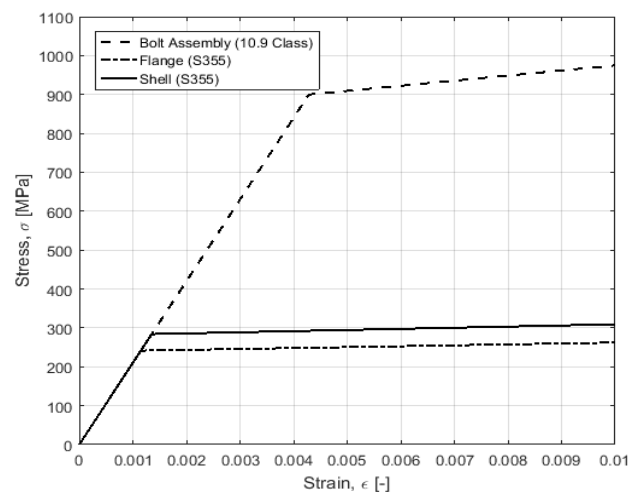

Figure 9. Definition of joint geometry.

Figure 10. Properties of bolt, head, nut, washers (bolt assembly), shell and flange materials.

Table 3. Geometrical and material parameters.

Description	Symbol	Value	Unit
Outer diameter of shell	OD	6	[m]
Nominal shell thickness	t_s	0.08	[m]
Nominal flange thickness	t_f	0.18	[m]
Nominal flange width	b_{ges}	0.31	[m]
Dist. bolt center to flange edge	a	0.15	[m]
Dist. bolt center to shell center	b	0.12	[m]
Inner radius	r_i	15	[mm]
Number of bolts	n_b	140	[-]
Nominal bolt size	d_{nom}	64	[mm]
Nominal diameter of washer	d_w	115	[mm]
Nominal washer thickness	h	10	[mm]
Grip length	l_g	380	[mm]
Nominal bolt length	l_{nom}	450	[mm]
Shank length	l_{sch}	332	[mm]
Cross section area of shank	A_{sch}	3,217	[mm^2]
Cross section area of bolt thread	A_{bd3}	2,520	[mm^2]
Nominal diameter of washer	d_w	115	[mm]
Characteristic yield strength of shell (t=80mm)	$f_{yk,sh}$	325	[MPa]

4.2. Analytical approach
ULS and FLS resistance of the L segment are found analytically in this section.

4.2.1 Ultimate limit state: The analytical ULS determination of the L segment joint is carried out according to Section 2.1. The found tensile resistance of the L segment and bolt configuration using the corresponding equilibrium equations is summarized in Table 4. The L segment is seen to exhibit a load deformation characteristic leading to failure mode B. Indicating development of a plastic hinge in the flange at the transition to the shell and subsequently tensile failure of the bolt. Equivalent design ULS loads at the MP-TP joint from a COWI A/S OWF project are presented in Table 5 including the tensile equivalent normal force determined from Equation (1). The utilization ratio representing the ratio between the equivalent tensile normal force and the resistance of the L segment is presented in Equation (18).

$$UR_Z = \frac{F_z}{F_{ult}} = 0.88 \tag{18}$$

4.2.2 Fatigue limit state: The analytical FLS determination of the L segment according to Section 2.2 is limited to an investigation of the cyclic loads in the bolt during operation of the WTG. Parameters for establishment of the Schmidt-Neuper curve reflecting the bolt force as a function of the tensile

force in the shell wall are presented in Table 6. The spring stiffness of the bolt assembly and L-segment under compression are specified according to procedures in [10].

Table 4. Tensile resistance for failure mode a-c for the l flange single bolt connection.

Description	Symbol	Value	Unit
Plastic limiting moment of flange without hole	M_{pl2}	334	[kNm]
Plastic limiting moment of flange with hole	M'_{pl2}	150	[kNm]
Plastic limiting moment of tubular section	M_{pl3}	56	[kNm]
Design value of limit tension force	$F_{t,Rd}$	1,927	[kN]
Limit tension force failure mode A	$F_{U,A}$	1,927	[kN]
Limit tension force failure mode B	$F_{U,B}$	1,279	[kN]
Limit tension force failure mode C1	$F_{U,C1}$	1,980	[kN]
Limit tension force failure mode C2	$F_{U,C2}$	2,448	[kN]

Table 5. Resulting ULS design loads for full flange and segment model

Global design bending moment	Global design Axial force	Equivalent normal force
$M_{Ed} [kNm]$	$N_{Ed} [kN]$	$F_z [kN]$
248,475	10,674	1,123

Table 6. Parameters for definition of bolt force as function of tensile force in shell wall.

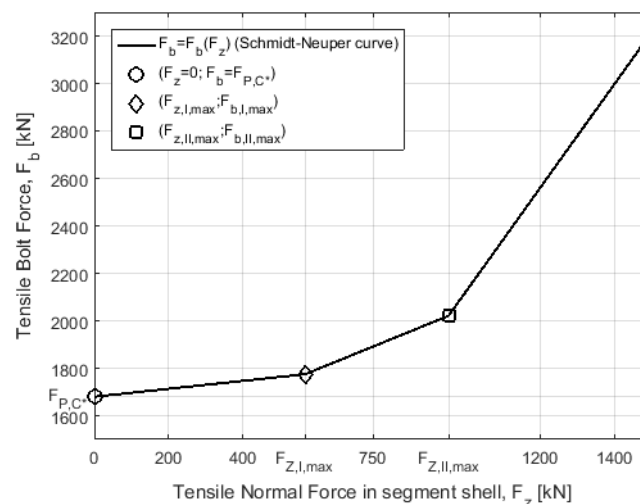| Description	Symbol	Value	Unit
Spring stiffness, bolt	p	0.17	[-]
Spring stiffness, clamped flange	q	0.83	[-]
Design preload	$F_{p,C*}$	1,680	[kN]
Shell force max. limit (region 1)	$F_{z,I,max}$	568	[kN]
Shell force max. limit (region 2)	$F_{z,II,max}$	954	[kN]
Bolt force max. limit (region 1)	$F_{b,I,max}$	1,775	[kN]
Bolt force max. limit (region 2)	$F_{b,II,max}$	2,021	[kN]
Auxiliary parameter	$\lambda*$	2.1	[-]

Figure 11. Characteristic tensile bolt force as a function of the shell force by the Schmidt-Neuper approach. Figure modified from [7].

The trilinear relation between shell- and bolt force for the segment flange is presented in Figure 11. The tensile shell force, F_z, is determined from Markov matrices containing information on the moment

load cycles at the MP/TP joint due to the cyclic actions on the foundation. The Markov matrix containing the governing directional cyclic loads relative to north is used as basis for the verification. The moment loads in the Markov matrix are sorted into bins, j, based on the magnitude of the moment range. Each bin contains n_i number of load cycles. The extent of the Markov matrix used in this paper is given in the format presented in Table 7. The Markov matrix includes information on min. and max. moment ranges and min. and max. mean moment values for the load cycles included in each bin [13]. The Markov matrix contains $9.95 \cdot 10^8$ load cycles divided into $j = 5,373$ bins which in this study are assumed to reflect the expected load history for the foundation.

From the information in the Markov matrix the min. and max. values of the shell force are obtained by Equation (19) to (24). A_{shell} is the cross sectional area of the shell for the L segment, $W_{E,shell}$ the section modulus of shell, and A_{bd3} the minor cross section area of the bolt at the thread-root section.

Table 7. Markov matrix incl. bending moments and number of cycles sorted into bins. Example values given in top row.

Min. moment range $\Delta M_{min,j}$ [kNm]	Max. moment range $\Delta M_{max,j}$ [kNm]	Min. mean moment $M_{mean,min,j}$ [kNm]	Max. mean moment $M_{mean,max,j}$ [kNm]	No. of cycles $n_{j,I}$ [-]
0	$1.398 \cdot 10^3$	$-1.053 \cdot 10^5$	$-1.036 \cdot 10^5$	9
$\Delta M_{min,2}$	$\Delta M_{max,2}$	$M_{mean,min,2}$	$M_{mean,max,2}$	n_2
$\Delta M_{min,3}$	$\Delta M_{max,3}$	$M_{mean,min,3}$	$M_{mean,max,3}$	n_3
$\Delta M_{min,4}$	$\Delta M_{max,4}$	$M_{mean,min,4}$	$M_{mean,max,4}$	n_3

$$\Delta M_{mean,j} = \frac{\Delta M_{min,j} + \Delta M_{max,j}}{2} \tag{19}$$

$$M_{m,j} = \frac{\Delta M_{mean,min,j} + M_{mean,max,j}}{2} \tag{20}$$

$$\Delta F_{z,j} = A_{shell} \cdot \frac{\Delta M_{mean,j}}{W_{E,Shell}} \tag{21}$$

$$F_{z,mean,j} = A_{shell} \cdot \frac{M_{m,j}}{W_{E,Shell}} \tag{22}$$

$$F_{z,\max,j} = F_{z,mean,j} + 0.5 \cdot \Delta F_z \tag{23}$$

$$F_{z,\min,j} = F_{z,mean,j} - 0.5 \cdot \Delta F_z \tag{24}$$

The non-linear dependency of the shell force and the bolt force illustrated in Figure 11 result in the maximum and minimum tensile bolt force being determined for each bin. The stress range in the bolt is found according to Equation (25) to (27) for the minor cross section area of bolt, A_{bd3} considering the reduction of the bolt diameter due to the thread.

$$\Delta F_{b,j} = F_{b,\max,j} - F_{b,\min,j} \tag{25}$$

$$\Delta \sigma_{b,max,j} = \frac{F_{b,max,j}}{A_{bd3}} \qquad \Delta \sigma_{b,min,j} = \frac{F_{b,min,j}}{A_{bd3}} \tag{26}$$

$$\Delta \sigma_{b,j} = \left| \Delta \sigma_{b,\max,j} - \Delta \sigma_{b,\min,j} \right| \tag{27}$$

The sum of the fatigue damage in the bolt is based on the S-N approach in [9] under assumption of linear cumulative damage (Palmgren-Miner rule):

$$D = \sum_{i=1}^{j} \left(\frac{n_i}{N_i} \right) \le 1.0 \tag{28}$$

As bending moments in the bolt are not considered, the detail category reference strength of the bolt, 36* (40 MPa) is used for damage accumulation according to [5].

Available S-N curves are limited to nominal bolt sizes up to 30mm. The M64 bolts studied in the present paper exceeds this value, hence the additional size effect leading to a reduction of the fatigue strength, is to be considered. Multiplying the reduction factor, k_s defined in Equation (29) with the reference strength of the bolt account for this effect according to [5].

$$k_s = \left(\frac{30}{d_{nom}} \right)^{0.25} \tag{29}$$

The obtained fatigue damage for the bolt exposed to the loads presented in the Markov matrix result in a summarized fatigue damage in Equation (30).

$$\sum D_{bolt} = 0.83 \le 1.0 \tag{30}$$

4.3. Numerical approach
The ULS and FLS capacity for the numerical L flange model are determined. The model includes the flange with connected shell, bolt and washer. The equivalent normal force is defined as a variable pressure load applied at the top of the TP shell.

4.3.1 Ultimate limit state: The maximum allowable tensile load, $f_{ult,}$ according to the analytical approach in Section 2.1 is applied as reference in the numerical analysis to obtain the corresponding stresses and plastic strains. Using this approach result in the safety level inherent in the analytical solution are ensured in the numerical segment model. Positions A-E in Figure 12 are selected for the analysis as they represent the points of interest for failure mode B.

The calculated axial stresses in the bolt and the flange segment, for the segment force equal the analytically derived ultimate resistance, are presented as contour plots in 0 and 0. Stresses and plastic strains as a function of the segment shell force for positions A-E are given in Figure 15 and Figure 16. The obtained maximum allowable plastic strains are listed in Table 8.

The development of plastic strain shown in Figure 16 indicates that the elastic limit is exceeded for a tensile segment force equal to 1,100kN and consequently a overutilization according to Equation (31).

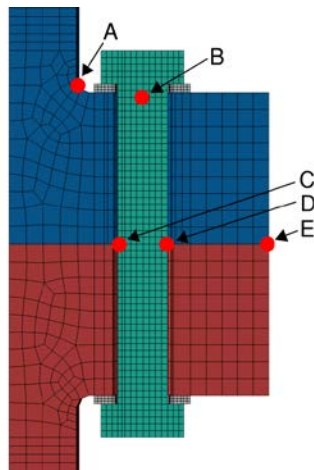$$UR_{elastic} = \frac{F_{z,elastic,max}}{F_{ult}} = 1.16 \tag{31}$$

Figure 12. L segment model geometry incl. idealized MP/TP flanges, equivalent bolt diameter, identical bolt head and nut, and washers. Pos. A-E indicate investigated positions.
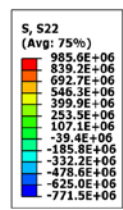
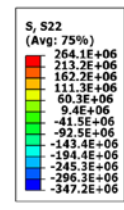**Figure 13.** Axial stresses in the bolt for $F_z = F_{ult}$

Figure 14. Axial stresses in the shell and flange for $F_z = F_{ult}$
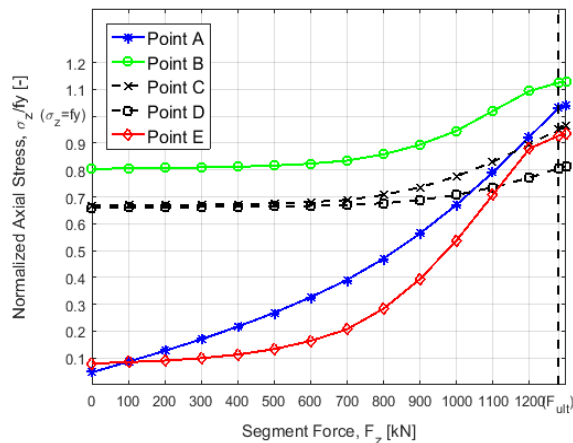

Figure 15. Normalized axial stresses at pos. A-E as function of tensile shell segment force.
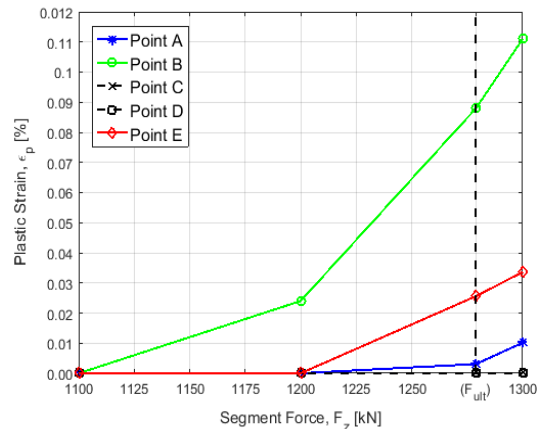
Figure 16. Plastic strain at pos. A-E as function of tensile shell segment force.

Table 8. Max. allowable plastic strains for positions A-E.

Position	Max. Plastic strain [%]
A	0.003
B	0.088
C-D	0
E	0.026

4.3.2 Fatigue Limit State: The fatigue capacity of the bolt is investigated by a finite element analysis (FEA) of the bolt center, positions C-D, and near the transition from bolt head to shank, position B shown in Figure 12. The segment shell force is defined in the numerical model for a range of -1,000kN to 1,500kN, covering the full load range of the Markov matrix.
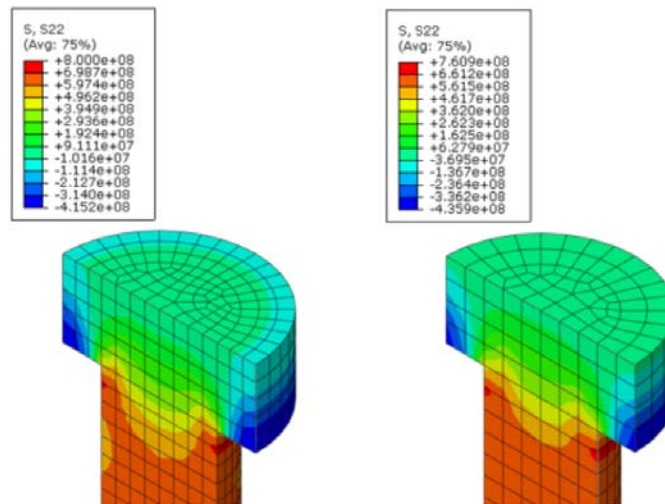
Figure 17. Output stresses for Fz = 600kN for a mesh size of 8mm and 10mm. Figure from [7].

The stresses obtained from the FEA at the bolt center and near the bolt head are extracted for the defined segment load range and for two mesh configurations as illustrated in Figure 17.

The position-specific bolt stresses as functions of the shell force are utilized to determine the stress range for each load bin in the Markov matrix according to (28). The stresses are hereby a function of the obtained relation between the segment and bolt force, shown in Figure 18. Damage accumulation is calculated equivalent to Section 2.2, except that a detail category reference strength of 50 MPa is chosen. This is a consequence of the numerical model considers both axial and bending stresses. The fatigue damage sum is given in Table 9.

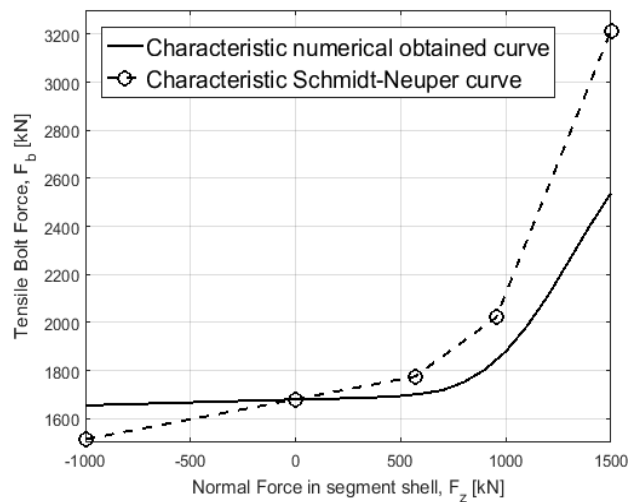**Figure 18.** Characteristic tensile bolt force as a function of the shell force in the segment shell wall. The normal force range covers all load values derived from the Markov matrix.

Table 9. Accumulated fatigue damage in the bolt for two element sizes

	Fatigue damage (element = 8 mm)	Fatigue damage (element = 10 mm)
Bolt head	0.36	0.04
Bolt Shank	0.041	0.028

5. Comparison and discussion

The analytical and numerical results of the L flange segment are compared and discussed in the following.

5.1. Ultimate limit state

The minimum derived tensile resistance in Table 4 is obtained for failure mode B. The computed stresses shown in Figure 13 and Figure 14 confirm this behavior. As seen at the transition of the pile wall to the flange, local yielding develops and subsequently load transfer via the inner edge of the flanges at the limit tension force of the bolt. As a result positions A-E, defined in Figure 12, are specified as hot spots for establishing a link between the tensile shell resistance and the corresponding stresses and plastic strains. From the comparison of the analytically and numerically obtained results in positions A-E the following is highlighted:

- Maximum stresses and corresponding development of plastic strains are obtained at point B in Figure 15 and Figure 16. The presented result indicates that a more detailed study of the stresses in this area is needed along the entire circumference.
- As the tensile segment force shown in Figure 15 increases the slope of the compressive stresses, representing the prying force, at (pos. E) develop more rapidly. As result, the slope of the graphs for the tensile stresses in the bolt (pos. B-D) becomes steeper. As the analytical approach does not include any tolerances, the prying force presented in Figure 15 is seen as minimum value.
- The difference in stress found at the two sides of the bolt C-D in Figure 15 is seen to increase with increasing tensile segment load. The difference is explained by the fact that the secondary bending moment in the bolt is not considered in the analytical approach.
- The plastic strains obtained in Table 8 are the answer to an extended requirement that ensures the integrity of the connection according to the analytical approach. As the analytical L flange concept ignores the fact that opening of the connection and plastic deformation will lead to some redistribution of forces, this requirement is to be maintained for verification of a full flange model.

5.2. Fatigue limit state

The numerically determined accumulated fatigue damage sum in the bolt is found by the numerical approach to be approximately 50% lower than the analytically obtained value. Furthermore, the numerical model indicates that the maximum fatigue damage in the bolt occurs in the bolt shank near the bolt head. The difference between the analytically and numerically obtained fatigue damage is seen to be caused by:

- Figure 18 shows the numerically and analytically derived bolt forces as a function of the segment shell force. For a given tensile shell force it can be seen that the numerically predicted bolt force is significantly lower than the analytically predicted.
- The result shows the effect of the built-in fabrication tolerances in the Schmidt-Neuper method which are not included in the numerical model.
- An initial study of the fabrication tolerances identifies the estimated contact surface between two flanges as a crucial parameter for the slope of the curve.
  Using the numerical model as an alternative to the analytical approach includes consideration of following:
- The numerically obtained damage values are seen to be very sensitive to the mesh size. In order to directly apply the stresses obtained in the numerical model further investigations are required. In addition, the impact of simplifying the model bolt geometry should be clarified.
- The numerical procedure is as consequence found only to be applied for specification of the relation between segment shell force and the bolt force. Following this approach the integrity of the bolt can be verified for fabrication tolerances exceeding the values included in the Schmidt-Neuper method or sought optimized by consideration of the full flange model.

6. Conclusion

An analytical and numerical ULS and FLS examination of the L flange segment is presented as the basis for the ongoing development work on the design of the bolted MP/TP steel ring flange connection. The L flange segment is investigated due to the availability of analytical approaches making it possible to establish numerical criteria applicable to a full flange model. The analytically determined failure mode B in the analytical ULS determination is confirmed by the identical numerical model leading to the conclusion that the derived tensile resistance can be applied to specify plastic strain criteria. However, as the analytical approach does not consider tolerances, the tolerances influence on the plastic strain values is required before the criteria can be applied to a full flange model. Fabrication tolerances are included in the analytical FLS determination by the trilinear curve relating the segment force with the tensile bolt force. Comparison of the analytically and numerically determined accumulated fatigue damage shows the damage found by the numerical approach (which does not include tolerances) too low. Furthermore, the local obtained stress values in the numerical model are very sensitive to the choice of element size as well as the level of detailing of the bolt. The numerical FLS approach is therefore suggested to be preferred for determining the relation between the segment load and the tensile bolt force. Implementation of the numerical FLS model to a full flange model will require that sufficient fabrication tolerances can be included in the numerical model.

The presented results indicate that focus for future development work must include handling fabrication and installation tolerances in the numerical models.

References

[1]   Wind Europe 2017 *The European Offshore Wind Industry – Key Trends and Statistics 2016* vol 1, ed Pineda I and Tardieu P (Belgium: Wind Europe) p 7

[2]   Vries D 2010 *Offshore Monopile Failure – A solution may be in sight Windpower* [Online]. Available: http://www.windpowermonthly.com/article/1011507/offshore-monopile-failure---solution-may-sight

[3]   Offshore Wind Industry 2016 *Waiting for new tenders* number 2, ed Buddensiek V (Germany: Offshore Wind Inustry) p 24

[4]   Damiani R R 2016 *Offshore Wind Farms: Technologies, Design and Operation* vol 1, ed Chong Ng and Ran L (United Kingdom: Woodhead Publishing) chapter 10 pp 263-357

[5]   IEC 61400-6 2016 *Wind Energy Generation Systems – Part 6: Tower and Foundation Design Requirements*

[6]   Petersen C 2013 *Grundlagen der Berechnung und baulichen Ausbildung von Stahlbauten* vol 4, ed Harms R and Prenzer A (Munich: Springer Vieweg) chapter 16 pp 1165-1260

[7]   Thage K J 2017 *Investigation of Flange Connection Capacity for Offshore Wind Turbine Foundations* M.Sc. Eng. Thesis (Lyngby: Technical University of Denmark)

[8]   DiBt 2012 *Richtlinie für Windenergieanlagen Einwirknungen und Standsicherheitsnachweise für Turm und Gründung*

[9]   GL COWT 2012 *Guideline for the Certification of Offshore Wind Turbines, Rules and Guidelines, IV-Industrial Services, Part 2, Guideline for the Certification of Offshore Wind Turbines*

[10]   VDI 2230-1 2015 *Systematic Calculation of High Duty Bolted Joints – Joints with One Cylindrical Bolt*

[11]   DASt 021 2013 *Schraubenverbindungen aus Feuerverzinkten Garnituren M39 bis M72 entsprechend DIN 14399-4, DIN EN 14399-6*

[12]   DNVGL-RP-C208 2016 *Determination of Structural Capacity by Non-linear Finite Element Analysis Methods*

[13]   Hobbacher A F 2016 IIW-2259-15 2016: *Recommendations for Fatigue Design of Welded Joints and Components* vol 2, ed Mayer C (Switzerland: Springer International Publishing) chapter 10 pp 113-138